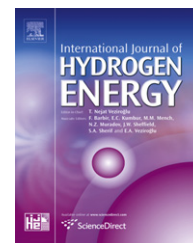


Available online at [www.sciencedirect.com](http://www.sciencedirect.com)

SciVerse ScienceDirect

journal homepage: [www.elsevier.com/locate/he](http://www.elsevier.com/locate/he)

# In situ measurement of temperature distribution within a single polymer electrolyte membrane fuel cell

Hong Lin, Tao-Fen Cao, Li Chen, Ya-Ling He, Wen-Quan Tao\*

Key Laboratory of Thermo-Fluid Science & Engineering of MOE, School of Energy & Power Engineering, Xi'an Jiaotong University, Shaanxi, China

## ARTICLE INFO

### Article history:

Received 1 March 2012

Received in revised form

30 April 2012

Accepted 8 May 2012

Available online 19 June 2012

### Keywords:

Proton exchange membrane fuel cell

Temperature distribution

Simultaneous measurement

Dynamic behavior

Temperature rise

Non-uniformity

## ABSTRACT

A novel test scheme for in situ measurement of temperature within a single polymer electrolyte membrane fuel cell (PEMFC) is proposed, which possesses the following attractive features: measuring interference with the internal environment of the fuel cell is likely reduced to minimum; simultaneous measurements for local temperatures of both sides of the fuel cell are conducted with enough numbers of measurement locations; and the cell temperatures are controlled in relatively careful and stringent strategies. Thermal and electrical behaviors of the cell tested are investigated, including the local and averaged temperatures at the back sides of cathode and anode flow field plates (FFPs), the outlet currents, and their variations with the test time. It is found that both temperatures and outlet currents exhibit complex dynamic behaviors; and the rise of temperature and the non-uniformity of temperature distribution of the back sides of the two FFPs are not negligible.

Copyright © 2012, Hydrogen Energy Publications, LLC. Published by Elsevier Ltd. All rights reserved.

## 1. Introduction

Operating processes inside proton exchange membrane fuel cells (PEMFCs) are coupled processes of fluid flow, mass transport, heat transfer, charge transport and electrochemical kinetics, in which temperature can be considered as a straightforward indicator, since temperature is tied directly to almost all major transport phenomena taking place within PEMFCs. For example, temperatures are correlated closely with transport factors, such as saturation pressure [1], mole fractions in the mixture [2], species diffusivities [3], thermo-osmotic diffusivity [4], location of the gas–liquid interface [5], latent heat of phase change [6], cell resistance [7], open circuit voltage (OCV) [8], electrochemical reaction rate [9], and exchange current density [10]. So, the temperature issue, known as the thermal management, must not be lost sight of,

when we research on inherent operational mechanism or engineering applications of PEMFCs.

There do exist temperature gradients inside PEMFCs being operated [11–16], and the temperature distribution under cell running is one of the most useful information, which can be used to validate the increasingly complicated numerical models, to ultimately optimize the design or operation of a cell, and to avoid the occurrence of performance reductions (degradations) or damage due to heat. In a sense the deep understanding of temperature distribution characteristics of a single fuel cell is the basis for a successful thermal management of fuel cell stack [17–24]. Dozens of literature have grown up related to the experimental measurement of the temperature distribution of a single PEMFC since the year of 2003 [25].

Temperature measurement using thermocouples is commonly conducted by inserting thermocouples or

\* Corresponding author.

E-mail address: [wqtao@mail.xjtu.edu.cn](mailto:wqtao@mail.xjtu.edu.cn) (W.-Q. Tao).

micro-thermocouples into different locations within a PEMFC, such as at the interface of different layers (ribs/channels/gas diffusion layers (GDLs)/membrane) [11,26–28] and/or between double sheets of carbon papers or membranes [25,27], and/or inside or behind the flow field plate (FFP) [12,29–31]. On account of the fact that thermocouples are commercially easily available within complete ranges of specifications and such measurements might bring minimal impacts on overall performance of a cell, thermocouples are widely adopted in multiple test schemes of PEMFCs for different aims.

With the aid of those technologies based on micro-electro-mechanical-systems (MEMS) there are two main types of micro-sensors adopted in local temperature determinations, thin film thermistor (TFT) – a patterned thin film gold thermistor [32] and resistance thermal detector (RTD) [33–41]. Compared with thermocouples, the micro-sensors fabricated by MEMS-based technologies have obvious advantages of small size, accurate orientation, high sensitivity, high flexibility and robustness, mass-producibility and relatively free locations of measuring, so they are especially suitable for in situ temperature measurement for miniature PEMFCs. Furthermore, micro thermal sensors can conveniently be integrated with other sensors, such as those kinds of humidity [36,38–40] and voltage [34–36], or can be both as micro flow and temperature sensors [35]. So combined measurements can be made with these multi-functional sensors fabricated with the aid of MEMS.

As a wave length converting technique, infrared thermal imaging (ITI) can capture thermal radiations from various parts of an objective body and form a two-dimensional image [42]. The outstanding advantages of ITI technique are real-time and ability of giving temperature distribution of the whole surface, and visualizing hot spots or regions. Thus, ITI is especially suitable for measuring the external surface of the end plate. To obtain temperatures inside the cell by ITI, cell configurations of its cathode [42–48] or anode [49] must be modified in order to allow infrared light transmitting into the cell.

In addition, some other unconventional measurements for temperature are attempted to determine local temperature of PEMFCs, such as those methods based on tunable diode laser absorption spectroscopy (TDLAS) [50–53], bandgap (BG) sensors [54], in-fiber Bragg grating (FBG) sensors [55,56] and phosphor thermometry [57].

The information obtained from all above-mentioned measurement methods for local temperatures inside a PEMFC can enhance, in a certain degree, our understanding of the complicated process within PEMFCs. However, regarding the present state of PEMFC inner temperature measurement and the specific measurement techniques briefly mentioned above following two basic questions are not resolved properly, which strongly affect the reliability and applicability of the measurement results.

1. All invasive methods might disturb the local environment inside PEMFCs, and due to the specific dimensions of a PEMFC these local disturbances to the points of interest are most likely significant, resulting in unpredictable uncertainties of measured data. In some cases such disturbances are so strong that even the overall

performance of the tested PEMFC is changed. On the other hand for the non-invasive method, it always needs to reform cell structures, with one immediate result is that normal heat dissipations of cell are changed, causing local behavior (hence, local temperature) deviating from normal operations. In addition the temperature distributions measured by the non-invasive method often are not the point values; rather, they represent the average temperatures over the paths along which the information is collected.

2. In the exiting literature there is no uniform and strict definition about the test states of PEMFCs, including the test time and the control strategies of the cell temperature, which vary from test to test. This situation can be witnessed from the following two facts. First, according to Refs. [58–62], steady state multiplicity in a PEMFC was evident, where investigations were conducted in an “idealized” experimental fuel cell - stirred tank reactor (STR). Their results indicate that, the operating time may have fairly important effect on the state of the cell tested, especially when the steady performance is the focus of study. Second, control strategies of cell temperature with heating pads (or mats) and circulating water were two common methods adopted in the published literature. These two control strategies are featured by non-uniformity of the controlled temperature field, slow response and environment-susceptivity, which all will add up the uncertainty of thermal boundary conditions of the cell tested, resulting in difficulties of data sharing. Bad-reproducibility of test data in PEMFCs is a well-known fact, and the uncertainty in the boundary conditions may be one of the major reasons.

From the state of the art of the in-cell temperature measurement, it is the authors' consideration that the intractable problem of measuring temperature distributions of PEMFC should be conducted step by step with the data in each step having enough accuracy and reliability. To assure the reliability and accuracy of the measurement results the first step we can do is to measure the temperature distributions at the outside surfaces of the bipolar plates of anode and cathode. In such a measurement the disturbances from the measuring sensors can be reduced to minimum. On the other hand, in numerical simulations these two temperature distributions are often the boundary conditions [63–72], hence, test data will be very useful to the establishment of an accurate numerical model. In addition, time duration of the measurement should also be appropriately recorded so that the effect of operating time on the measured results can be shown.

As a preliminary work of the above thoughts, a novel test scheme for the outside surface temperature of the two bipolar plates within a single PEMFC is presented in this paper. In the following presentation, experimental methodology is described first, including the fuel cell tested, measurement method, experimental system, measurement procedure and experimental data reduction. Second, presentation and analyses of the results are conducted with emphases being put on thermal and electrical behaviors of the cell tested. Finally, some conclusions are drawn.

## 2. Experimental

### 2.1. Fuel cell tested

A commercially available single PEMFC was tested in this study, which has six parallel serpentine gas paths with reaction areas of 50 cm<sup>2</sup> approximately. The serpentine structure of the cathode flow field is presented in Fig. 1, whose flow channels were machined into a graphite plate with dimensions of 84 mm × 84 mm × 2 mm. In order to alleviate longitudinal thermal conduction in the plane, a relatively thin thickness of 2 mm was adopted for the FFPs. The depth of the flow channels is 1 mm, and the width of the channels and ribs both are 1.16 mm (see Fig. 1). Gas channels both in the cathode side and the anode side are six parallel serpentine paths with five passes, and gases are fed in partial counter-flow mode, where oxygen flows into the upper right and leaves from the bottom left, while hydrogen has the opposite flow path, as shown by solid or broken lines in Fig. 1. Besides, for convenience of data processing the numbers with circle denote the measurement positions of the thermocouples in the anode side along the hydrogen flow path, while the zones in cathode side are numbered by two-dimensional coordinate system according to the sensors in 10 × 10 uniform arrangement.

The MEA in the fuel cell consists of Toray O60 acted gas diffusion layers and an NRE212 film coated with 60%Pt/C, 0.4 mg/cm<sup>2</sup> of catalyst loading on each side, forming an active area of 7 cm × 7 cm. No other special treatments such as hot press or level up were taken for the membrane electrode assembly (MEA). The fuel cell was assembled through eight M6 screws, each with a uniform torque of 2 N m by a resistive force meter. The two end clampers of the fuel cell were made of anodized aluminum with dimensions of 12 cm × 12 cm × 2 cm. The two current collector plates with 2 mm in thickness were made of copper coated with gold.

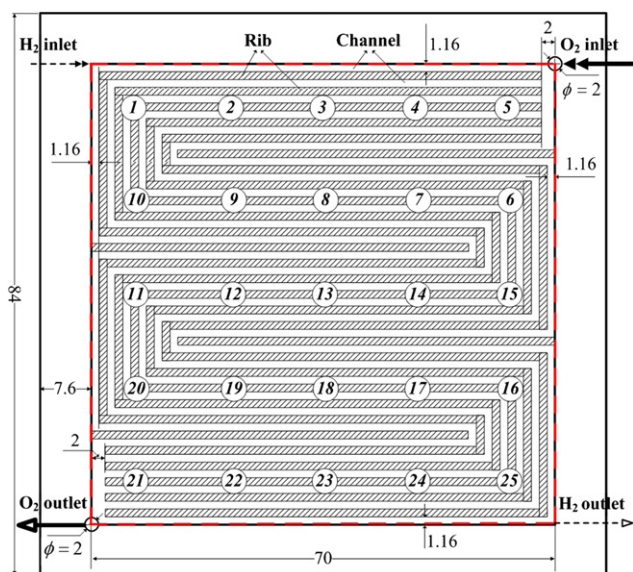


Fig. 1 – The serpentine structure of the cathode flow field plate (dimensions in mm).

### 2.2. Measurement method

Our major intention was to measure current density and temperature distribution of the outside surfaces of the bipolar plates of anode or cathode. Comparatively speaking, we were more interested in the current density of the cathode, so magnetic sensors with more expensive costs were used only on the cathode side, while cheaper thermocouples were used on the anode side.

Fig. 2 shows a schematic view of a cross section of the single PEMFC tested. It consists of seven integral components, i.e., an anode clumper (AC), an anode current collector (ACC), an anode flow field plate (AFFP), MEA, a cathode flow field plate (CFFP), a cathode current collector (CCC), and a cathode clumper (CC). Fig. 2 also illustrates the cross section structure of the specially designed test cell for measuring temperature distributions. In order to measure the temperature distributions of the back side of the AFFP, 25 holes in total with diameter of 1.8 mm each were drilled one by one through AC and ACC, through which thermocouples were inserted. Then, two 'O'-rings were set with tight fit in both ends of each shoulder holes across the clumper. By the two 'O'-rings thermocouple could be fixed and suspended in holes. Further, proper amount of heat conduction resin was squeezed between the thermocouple tips and the AFFP. Thermocouples in such settings could not only allow for good heat conduction to the AFFP, but also have fixed measurement locations, which would enhance the measurement precision and repeatability.

Thermocouples used in the anode were purchased from Omega Engineering, Inc., with tolerance class of 1 and precision of 0.5 °C claimed by manufacturers' specifications. The length and diameter of the thermocouple wire were 6 inch and 1/6 inch respectively. Preliminary calibrations were conducted in a thermostat water bath, in order to pick out thermocouples according to their precisions and stabilities. The thermostat water bath has a nominal precision of 0.1 °C and nominal stabilities of 0.01 °C with PID3 technique for controlling temperature, made in JULABO USA, Inc. (Julabo F26-ME). Readings of all 64 thermocouples submerged within the bath have been recorded for half an hour after the stabilization of the bath at a setting temperature, ranging from 5 °C to 95 °C with an interval of 5 °C. And then from 64 thermocouples 25 ones were picked out depending on their means and variances with time in half an hour. All these selected 25 thermocouples have stabilities of 0.2 °C. The maximum thermocouple

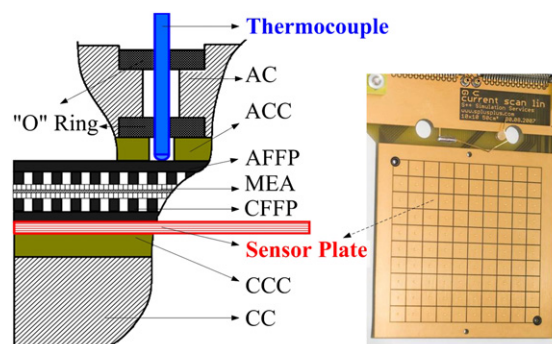


Fig. 2 – Schematic cross sections of the single cell.

conduction error in the measurement of surface temperature  $\Delta T_p$  is estimated as:

$$\Delta T_p = \frac{\lambda_2 \delta_1}{\lambda_1 \delta_2} \Delta T_{sh} = \frac{15 \text{ W}/(\text{m} \cdot \text{K}) \times 2 \times 10^{-3} \text{ m}}{25 \text{ W}/(\text{m} \cdot \text{K}) \times 152.4 \times 10^{-3} \text{ m}} (90^\circ \text{C} - 17^\circ \text{C}) = 0.575^\circ \text{C}$$

where  $\lambda_1$  and  $\lambda_2$  are the thermal conductivity of graphite plate [73] and the thermocouple wire (SS 304) [74], and  $\delta_1$  and  $\delta_2$  are the dimension of graphite plate and the thermocouple,  $\Delta T_{sh}$  is the maximum temperature difference between the environment and the inner measuring point.

Temperature measurement for the cathode was accomplished by a commercial Current Scan Lin (CSL) (Test 50), acquired from S++ Simulation Services, Germany. The test principle is based on the dependence of the permeability of a magnetically soft material on the magnetization and the temperature [75]. As shown in Fig. 2, a special sensor plate with 3.5 mm in thickness was inserted between CFFP and CCC. With gold plated this sensor plate has excellent conductivities for heat and electron transfer, and has a minimal impact on the operating of the cell tested. In the sensor plate there are 100 sensor units, each with an area about of 0.5 cm<sup>2</sup>. Soft ferrite material within the measuring units is strongly dependent on local temperature. The nominal accuracy of temperature measurement is 1 °C, and it takes 2 s to scan all 100 measuring units.

Generally, when the measurement of PEMFC temperature distribution was conducted, a reference point was often chosen in an FFP or an end plate on single side (typically referred to the cathode side). In such a situation, the cell temperature at one or both sides of the cell was controlled simultaneously by only a single measured temperature. One of the major purposes of this study was to investigate temperature profiles at both sides of a PEMFC, so we used two thermocouples, each at the center of the end plate in both sides as the reference point for each side. Thus, heating regulation of each side was separately conducted by single own temperature. In the previous studies commonly one or

two heating rods were used to heat the tested cell, while in the present experimental study eight heating rods (each with a power of 30 W) were placed evenly in the end plate. As a result, heat could transfer to the back side of FFPs homogeneously through the end plate with a large thickness of 20 mm, and uniform heat input to the fuel cell tested could be obtained.

It is important to mention that all sensors in our test scheme do not interfere with the gas pathway, and that the modification of cell design and component material is minimized. Further, due to the minuscule heat-conducting area percentage of the cross sections of the armored thermocouples array to the clamp (about 0.35%), by comparative experiments there was no sensible difference with and without armored thermocouples array in some general current–voltage polarization behaviors, and the maximum relative deviations of current did not exceed 0.4% at cell temperature of 60 °C, and 1.1% at 40 °C respectively. Hence the disturbances caused by the measuring sensors are expected to be at the least degree. The cell temperatures are controlled in relatively stringent strategies, with the back side temperatures measured and controlled separately on anode and cathode side. It took a comparatively long time of operating and measuring, 6 h in each case, so as to allow investigation on cell behavior variation with time.

### 2.3. The experimental system

The whole measurement process was conducted on Arbin Instrument modified for in situ temperature distribution measurement. Gas supply, electronic load and determination are controlled and monitored by a custom-built Arbin's FCTS. Arbin's FCTS is composed of several basic subsystems, including gas handling module, humidifier module, electronic load and PC-controlled flow/temperature/pressure module, cooling water handling module; for more details the website [76] can be referred. The schematic of the pertinent experimental test system is shown in Fig. 3. The accuracy of several key parameters of the Arbin Instrument is respectively 0.2 mV

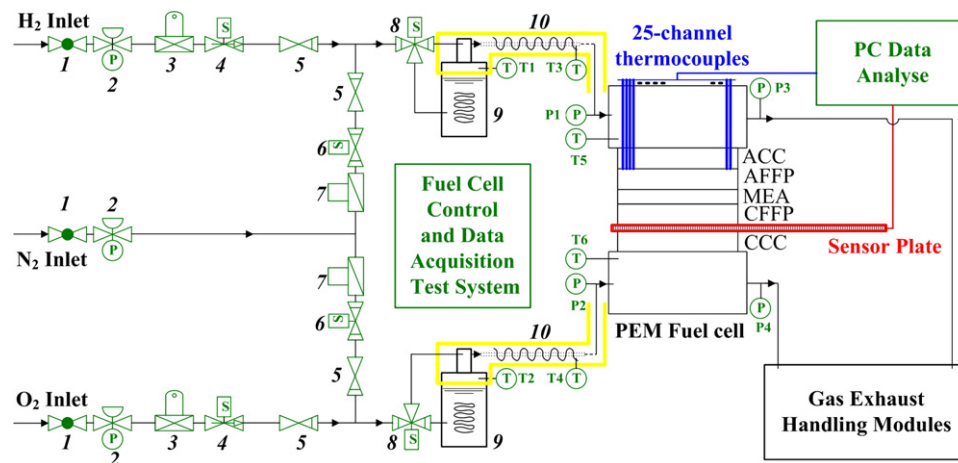


Fig. 3 – Schematic of experimental test system modified for in situ temperature distribution measurements (1-Plug valve, 2-Gas regulator, 3-Mass flow controller, 4-Solenoid valve, 5-Check valve, 6-Solenoid valve, 7-Gas rotameter, 8-3 Way solenoid valve, 9- Dew point humidifier, 10-Insulation cover).

for voltage, 0.01 s l pm for gas flow rate and 1 °C for temperature (T1–T6).

The PEM fuel cell was hung vertically in the air in a testing chamber, which was an enclosure in order to reduce the disturbances by the forced air convection in the lab. Four thermodetectors were placed in the chamber, respectively at a distance of about 30 cm right ahead of, rear of, upside of and underside of the test cell, whose average was taken as the environment air temperature. During the whole test process this environment temperature was kept almost constant, with a fluctuation about  $\pm 1.0$  °C. So the test environment could be regarded at a constant temperature.

#### 2.4. Measurement procedure and experimental data reduction

There are two common modes-potentiostatic (controlled voltage) and galvanostatic (controlled current) modes [77] to measure current–voltage behaviors in the test of fuel cell. One electrical variable is monitored while the other is controlled in both modes, which have respective advantages and disadvantages, used to different research cases. Constant current mode is preferable, when quantitative analysis is conducted directly related to current, while constant voltage mode is seemingly safe and reliable without our initial knowledge of the maximum current limitation. Therefore we use the constant voltage mode, and perform some qualitative analyses. It could not affect main conclusions drawn at the end. The main steps of the experimental procedure are as follows:

1. Establishment of identical initial state: Gas flow rates, back pressures and temperatures of both sides of gas lines, humidifiers and the cell were all monitored carefully under OCV conditions until all these parameters reached their pre-specified stable values. This process usually took about 1–2 h. The gas flow rates were kept at constant and the

cathode and anode stoichiometries were 4 and 2, respectively at two initial cell temperatures under the current density of 1 A/cm<sup>2</sup>. The inlet relative humidities of oxygen and hydrogen were 25% and 100%, respectively. All other running conditions can be found in Table 1.

2. Diminishing the effects of loading history: To further realize reproducible initial conditions the effects of loading history should be diminished. The tested cell was then kept at rest for about 1000 s after above operating conditions were reached. In the meantime, current outputs were calibrated by shutting CSL after 990 s.
3. Measurement of current density under constant voltage mode: The cell was loaded under pre-specified voltage setting from 0.9/0.8/0.7/0.6/0.5/0.4/0.3 V, and each measurement took 6 h. Sampling intervals for temperature distributions of the anode and the cathode were 1 and 2 s, respectively.
4. Temperature data reduction: Under each voltage set there were more than  $25 \times 23,600$  readings recorded for temperature. The temperature at any instant within the test period could easily be obtained by interpolation using calibration data from the data recorded.

In total, the cell performance was tested under 14 operating conditions and the time of all tests lasted up to 112 h approximately.

### 3. Results and discussion

#### 3.1. Anode average temperatures versus time

As indicated above, when the fuel cell was operated, under seven different constant voltages and two different initial temperature settings, the outputs of the 25 thermocouples at the back side of the AFFP were recorded, and the average value of which at the same moment was taken as the average temperature of the AFFP. The measured anode temperatures versus time are plotted in Fig. 4, where solid lines stand for cases of initial temperature of 60 °C, while dash lines for cases of 40 °C.

It can be seen from Fig. 4 that as a whole in most cases of the present output voltage there exists a marked abrupt change of the anode temperatures in the early stage, and the lower the preset outlet voltage, the larger the abrupt change, and the steeper the temperature gradient. This is because a lower voltage is associated with a stronger reaction intensity leading to a larger heat generation [78]. It is evident that if the test period is long enough, the anode temperatures can reach relatively stable values or fluctuate around some relative stable plateaus (the case of 40 °C/0.3 V). Exceptionally at voltages of 0.9 V and 0.8 V, anode temperatures maintain just about those preset initial temperatures of cell in all test time, due to low heat generation resulted from low outputs of overall current, meanwhile the heating pads (which were set in the cell and used to maintain the required initial cell temperature) may play some roles to keep the required temperature. When the cell temperatures exceed initial temperature settings appreciably, heating pads are shut down

**Table 1 – Experimental operating conditions.**

Items	Setting values	
O <sub>2</sub> flow rate (slpm)	0.876	0.798
H <sub>2</sub> flow rate (slpm)	1.036	0.845
O <sub>2</sub> inlet temperature, T4 (°C)	60	40
H <sub>2</sub> inlet temperature, T3 (°C)	60	40
O <sub>2</sub> humidifier temperature, T2 (°C)	32.6	15.7
H <sub>2</sub> humidifier temperature, T1 (°C)	60	40
Cathode end plate initial temperature, T6 (°C)	60	40
Anode end plate initial temperature, T5 (°C)	60	40
Cathode back pressure, P4 (psig)	14.70	14.70
Anode back pressure, P3 (psig)	14.70	14.70
Environment temperature (°C)	17 ± 1 °C	

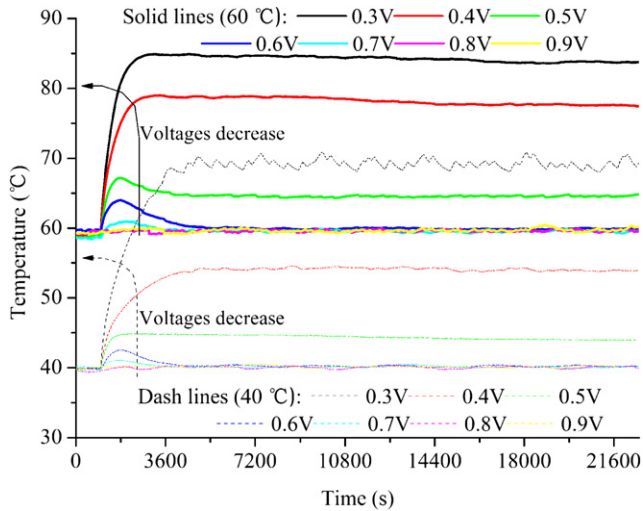


**Fig. 4 – Anode average temperatures as functions of test time under seven outlet voltages at two initial settings of cell temperatures.**

automatically, and thus the cell temperatures are kept wholly by heat generated in electrochemical reaction within the cell.

By carefully expecting the curves of temperature versus time till stabilization, two situations can be identified. As the first situation, temperature exhibits obviously overshoot before stabilization. This happens when output overall currents are moderate, such as voltages of 0.7 V, 0.6 V and 0.5 V under initial temperature of 60 °C, 0.7 V and 0.6 V under initial temperature of 40 °C. In these cases the anode temperatures increase sharply, reach some maximums, then reduce gradually and ultimately keep relatively stable values for long test time. For the initial temperature of 60 °C, the moment at which the temperature reaches the maximum is about 2030 s, 1790 s, and 1760 s for voltages of 0.7 V, 0.6 V and 0.5 V respectively, while under initial temperature of 40 °C both cases of 0.7 V and 0.6 V have peak temperatures at about 1800 s. Another situation is that temperatures of the anode do not show distinct overshoot as described above, but reach stabilization in asymptotic behavior over time. Such cases are voltages of 0.4 V, 0.3 V under initial temperature of 60 °C and 0.5 V, 0.4 V, 0.3 V under initial temperature of 40 °C.

In summary, substantial changes of anode temperatures with time can be seen during the onset of the voltage change; however, anode temperatures can reach relatively stable values or fluctuate around some relative stable plateaus, provided that the test period is long enough. Table 2 lists the time needed for anode temperatures to reach stable state (temperature stable time, or TST for short), from which we can find that the anode TST has the order of magnitude about half to 1 h, depending on the operating conditions. The time period within which a fuel cell can reach steady state is often called thermal time constant [30].

Physically it can be expected that the specific value of TST depends not only on the cell size but also on the location where this temperature is referred to. Generally, the larger the cell size is, the longer the TST is, and the TST of an inner component is shorter than that of the outside one. For

**Table 2 – The lapse of time for anode temperatures to reach the relatively stable state (temperature stable time, TST).**

	0.7 V	0.6 V	0.5 V	0.4 V	0.3 V
60 °C	3400 s	4600 s	3700 s	2400 s	2000 s
40 °C	2800 s	3500 s	1100 s	3300 s	2800 s

example, it is reported in the literature that a PEMFC with a small reaction area and simple flow paths had a thermal time constant of about 900 s [30], and the temperatures on the surface of membrane electrode assembly (MEA) also took about 900 s to become steady [37]. The literature also shows that temperatures could not be steady within 700 s due to the liquid water [57]. All these reference results accord with our observations qualitatively, thus at least in the order of magnitude our results are reasonable. The time constant of a high temperature PEMFC was estimated by using lumped-parameters dynamic equations in Ref. [79], however, the time constant of a low-temperature PEMFC has not been investigated systematically. It is, seemingly, first in the literature to provide such a detail measurement process for the cell temperature variation.

### 3.2. Output overall current versus time

Fig. 5 shows the overall current outputs varying with the test time under seven chosen constant voltages and two initial temperature sets, separately represented by solid lines and dash lines. It can be seen that low output of the overall currents can soon reach stable, while high output may fluctuate to some extent, presenting complex dynamic behavior.

To facilitate the comparison of these current change trends over time, dimensionless current will be used in the following discussion, which is defined as the real output current divided by the average value over the later 5 h. From temperature data presented above, the cell temperatures are found being above the initial setting obviously when the cell output voltages are

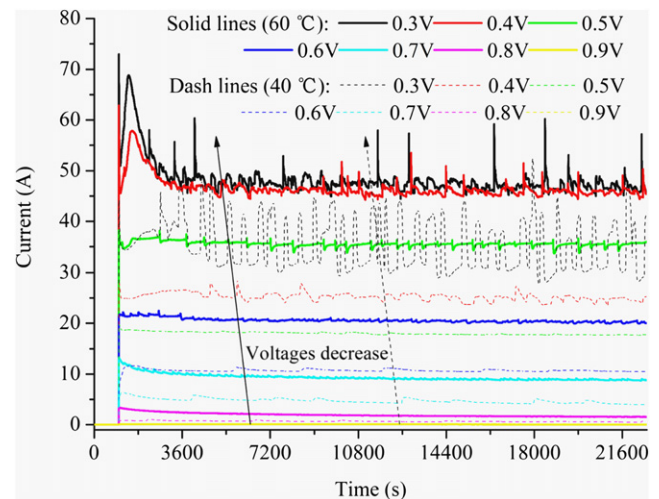


**Fig. 5 – Outlet overall currents as functions of test time under seven outlet voltages at two initial settings of cell temperatures.**

lower than 0.6 V, and heating pads are cut out automatically. In these cases the cell is self-heated without any external sources of heating. So we select cases with output voltage below 0.6 V for discussion.

Fig. 6 shows dimensionless current densities changing with time for 1 h just after setting the four different constant voltages. During the first 20 s or so, outlet currents overshoot (see the pictures at the right lower part of the figure) are obviously accompanied by the step change of voltages at 0.3 V, 0.4 V and 0.5 V, while at voltage of 0.6 V outlet currents increase relatively slowly without any overshoot. Dimensionless current densities of the overshoot are 1.5, 1.4 and 1.1 respectively at voltages of 0.3 V, 0.4 V and 0.5 V under initial temperature 60 °C, indicating that the more the relative voltage jump, the more currents overshoot. Dimensionless current density is close to 1.3 at 0.3 V under 40 °C, showing that the dimensionless current density under 60 °C is larger than that under 40 °C at the same voltage jump. The occurrence of the first current overshoot can be explained by the compulsion exerted by external electrical loading caused by the voltages-jump. The more the voltage jumps, the more important the compulsion is, hence, the more the overshoot comes forth. On the other hand, due to a ‘vacuum’ effect causing by ambient air flowing into the anode side from the exhaust pipe, some undershoot behavior of outlet currents always occur [80]. However, there is no-occurrence of undershoot in our test (the case at voltage of 0.6 V), and the possible reasons are as follows: Not air but hydrogen in the exhaust pipe with more than 20 m long in our test system flows back to the anode side; also, stoichiometry ratios used corresponding to ‘excess’ conditions may suppress the undershoot behaviors. After the very short first period the outlet currents vary with time very complicatedly, exhibiting coupled effects of charge transport and all other processes such as electrochemistry, flow and mass transfer processes. As a whole such variations exhibit somewhat periodic character. These periodic durations are mainly determined by the time scale of fluid redistribution. For example, according to [54] water distribution has time constant of the order of 100 s. As a whole the current variation characteristics with time for the cases

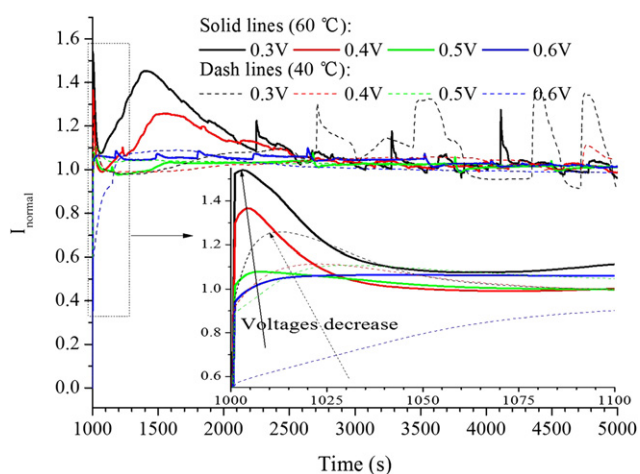
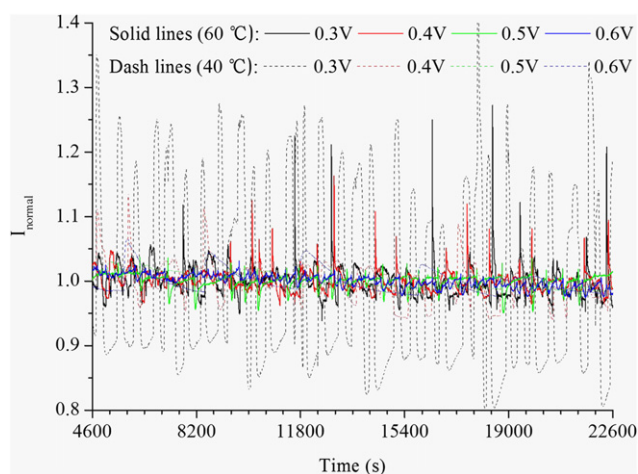


**Fig. 6** – Dimensionless current density as functions of test time during about 1 h just after voltage jump under four voltages at two initial settings of cell temperatures.

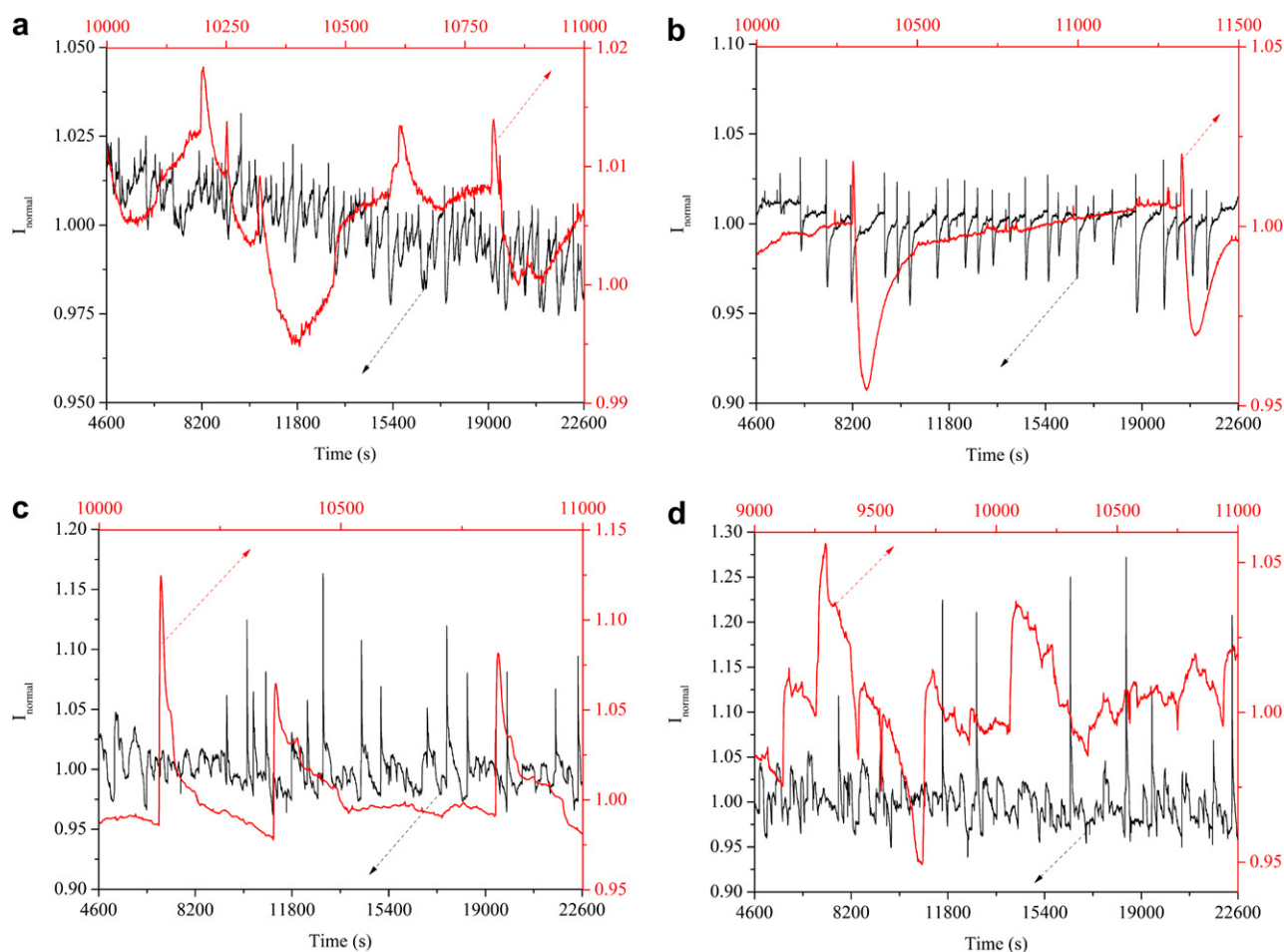
studied can be summarized as follows. At the initial temperature of 60 °C, currents at 0.3 V and 0.4 V vary with time from state of “overshoot” to some kind of “oscillation”; while at 0.5 V and 0.6 V, current level decreases gradually to reach the dimensionless current of 1.0 with much less oscillation amplitude; At the initial temperature of 40 °C currents at the four voltages vary from state of “gentleness” to “oscillation” with time. There is obvious current oscillation at voltages of 0.3 V, 0.4 V, 0.5 V and 0.6 V respectively at time of 1500 s, 3500 s, 4000 s, and 4500 s, before which dimensionless current keeps 1.0 approximately.

Fig. 7 shows how the dimensionless current densities change with time in the latter 5 h. It can be seen that the outlet currents fluctuate within a certain range for most cases, and under the same initial temperature, the lower the preset voltage, the more significant the fluctuation of the outlet currents. And under the same voltage the higher the initial temperature is, the more appreciable the fluctuation presents. For example, at the initial temperature of 60 °C the outlet current fluctuates between 0.9 and 1.3 at 0.3 V, while it fluctuates between 0.9 and 1.5 at 40 °C under the same voltage. These outlet current oscillations exhibit some rough periodic trends, and two obvious cases are those at 0.5 V under 60 °C with average interval of 650 s to 750 s and those at 0.4 V under 40 °C with average interval of about 550 s. Formation, accumulation, and expulsion of liquid intermittently are supposed to be the causes of above current behavior. Similar observations are found in [81] with two differences: firstly, interval time of fluctuation is shorter in [81], and small reactive area (5 cm<sup>2</sup>) tested may be the cause. Secondly, current fluctuation range is wider at higher voltages in [81], and operation with hydrogen and oxygen under not fully humidified condition may explain this. Cell gases fed in our test are fully humid hydrogen and partially humid oxygen which is one of the most common operating conditions in the references. Under our cases, dynamic changes of outlet current with time are also found when the fuel cell is operated for several hours, still exhibiting some dynamic behavior such as oscillations.

To further examine above current dynamic behaviors in detail, Figs. 8 and 9 show enlarged information of the current



**Fig. 7** – Dimensionless current density as functions of test time during the latter 5 h under four voltages at two initial settings of cell temperatures.



**Fig. 8 – Dimensionless current density as functions of test time during the latter 5 h overlapped with enlarge views during small durations at four voltages under 60 °C initial temperature: a) 0.6 V; b) 0.5 V; c) 0.4 V; d) 0.3 V.**

oscillation for two different time scales with the red ones having a larger enlargement ratio corresponding to the right and top coordinate axes. These current oscillations are clearly not all the same, which might be attributed to different local environments according to different outlet voltage and different cell initial temperature settings. It is speculated that at the same given macroscopic conditions (i.e., the same initial temperature and preset voltage) there exists different local environments inside the PEMFC tested which has six parallel serpentine gas channels and the reactive area of 50 cm<sup>2</sup>. In general, the local environment variation may be imaged as follows. When water is produced more and more, humidity of the membrane and thus the conductivity of proton become better and better, so the outlet current increases gradually (Fig. 8-a/d, Fig. 9-c/d). However, when water by drainage exceeds that produced in reaction, the outlet current will decrease (Fig. 8-a/c/d, Fig. 9-a/b/c). Or when more and more water accumulates inside the cell such that mass transfer is hindered, the outlet current will also decrease. If water accumulation ultimately results in flooding, the outlet current reduces sharply (Fig. 8-b). Meanwhile the pressure built-up by flooding in gas channels may drive water away from gas paths suddenly; consequently, the outlet current will increase steeply (Fig. 8-b/c, Fig. 9-a/b). All the

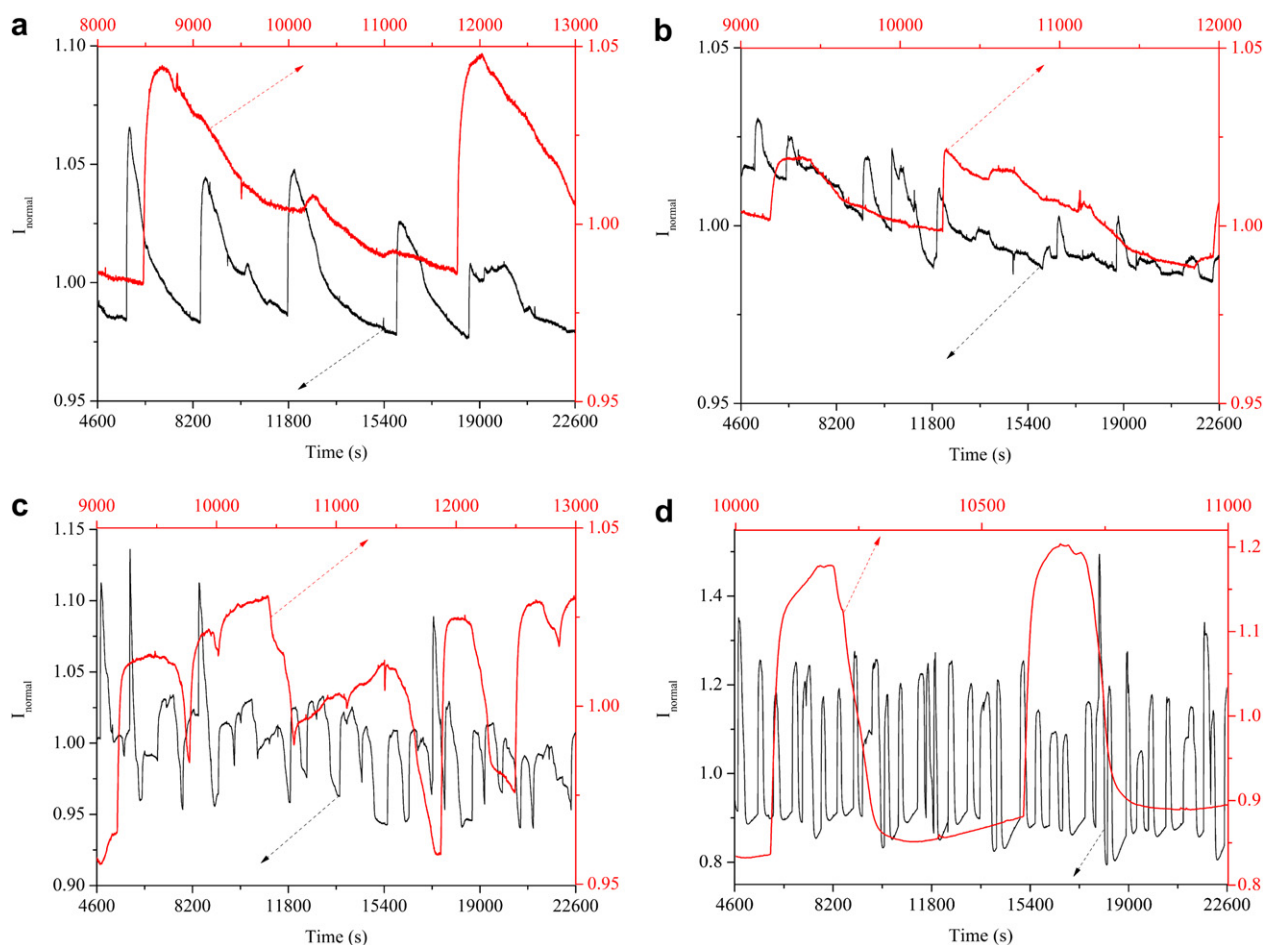
above gradual changes or sharp variations of the outlet currents can be found in Figs. 8 and 9. It is interesting to point out that the current variations with time at 0.3 V under 40 °C are very similar with those reported in [82].

Fig. 10 shows the relations between the outlet currents and anode temperatures for two representative cases of 0.5 V, 60 °C and 0.3 V, 40 °C. As expected, due to the thermal inertia cell temperature increases with outlet current (or vice versa). There is hysteresis between temperatures and currents: in the case of 0.5 V, 60 °C (Fig. 10-a) the temperatures lag behind the currents about 10 s and 100–200 s while currents go higher and lower, respectively, while in the case of 0.3 V, 40 °C (Fig. 10-b), these lag times are 100 s–200 s when the temperatures increase, and 400–500 s when they decrease.

### 3.3. Polarization behaviors and average temperatures at different voltages

The cathode averaged temperatures are obtained from 100 sensing cores of soft magnetically material at the cathode side. The average temperatures of the anode and cathode ( $T_c$ ,  $T_a$ ), overall current densities and outlet voltages are plotted in Fig. 11. Some general polarization behaviors can be observed from the figure, where the activation, resistance and





**Fig. 9 – Dimensionless current density as functions of test time during the latter 5 h overlapped with enlarge views during small durations at four voltages under 40 °C initial temperature: a) 0.6 V; b) 0.5 V; c) 0.4 V; d) 0.3 V.**

concentration polarizations can be distinguished. At a voltage of 0.3 V the current density reaches about 1.0 A/cm<sup>2</sup> and 0.7 A/cm<sup>2</sup> for initial temperatures of 60 °C and 40 °C, respectively, and the performance at initial temperature of 60 °C is better than that of 40 °C. The concentration polarization loss at initial temperature 60 °C can be clearly observed, caused by severe flooding resulted by too much water production at higher current densities. It is reasonable to expect that the integrated performance of the tested cell could be improved further, by means of optimization of operation conditions, or some conventional special treatments for the MEA and GDLs, but these are beyond the scope of this study.

At low current densities, averaged temperatures of both the anode and cathode basically remain their initial levels; however, they increase gradually with current densities from moderate to high values. The maximum averaged temperatures of the cathode and anode side can reach about 83 °C and 84.2 °C at initial temperature of 60 °C, respectively, being 23–24 °C higher than the initial. While at initial temperature of 40 °C those maximum values are 69.4 °C and 69.2 °C respectively with an increase about 29–30 °C. From these results it may be expected that the global temperature of a PEMFC may climb significantly under some operation conditions if no effective techniques are adopted to cool the

cell, then as a result, the fuel cell may operate at conditions deviating significantly from those expected. In such cases the polarization curve characterizing overall performance is formed with rising cell temperature, which undoubtedly brings uncertainties in the test data. Such a situation will be more serious for a fuel cell with a larger active area. From Fig. 11, it is also found that the average temperatures of the anode and cathode are very close to each other with a difference of 1–2 °C, which is slightly greater than those findings about the temperature differences between the two surfaces of MEA in [26], where coolant channels were utilized.

Attention is now turned to examine the relation of current densities and temperatures of different cell components. Following information is collected from existing literature. For cathode GDL surface temperatures there are logarithmic relations (i.e., temperature-logarithmic of current density) for high humid conditions and exponential ones for low humid conditions [57]; For the membrane temperatures, quadratic relations (i.e., temperature-quadratic of current density) for current densities less than 1 A/cm<sup>2</sup> and asymptotic relations for current densities greater 1 A/cm<sup>2</sup> [25]; For the cathode catalyst temperatures, linear relations with different slop at different gas flow rates are found in [28], while temperatures of all four interfaces are almost second order polynomial of

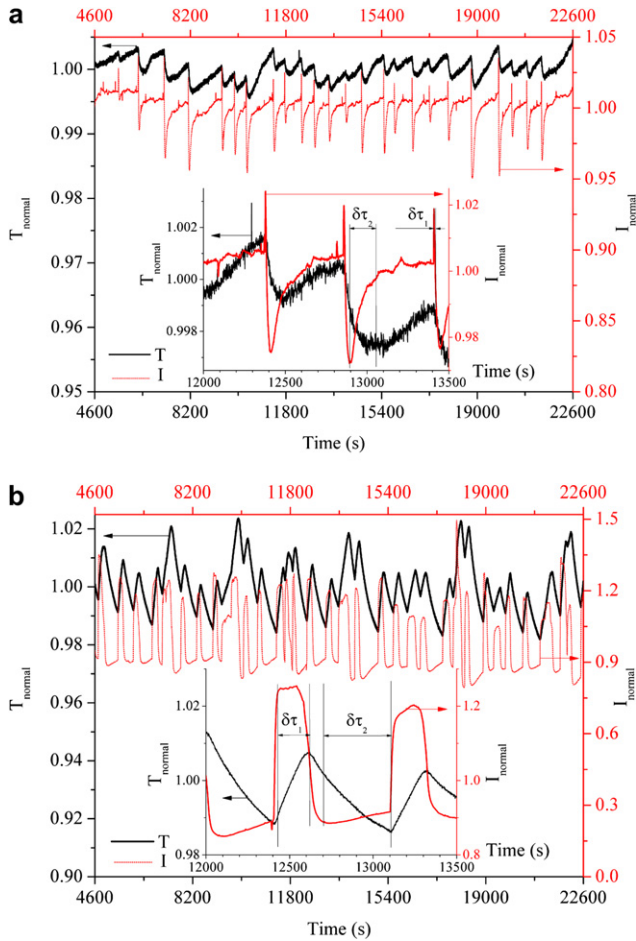


**Fig. 10 – Correlations between outlet overall dimensionless current density and dimensionless temperature: a) 0.5V/60 °C; b) 0.3V/40 °C.**

the current density can be found in [11]. In our test data it is found that the temperatures at the back sides of FFPs, both increases with current densities in somewhat quadratic relations. From the above observed results it can be seen that

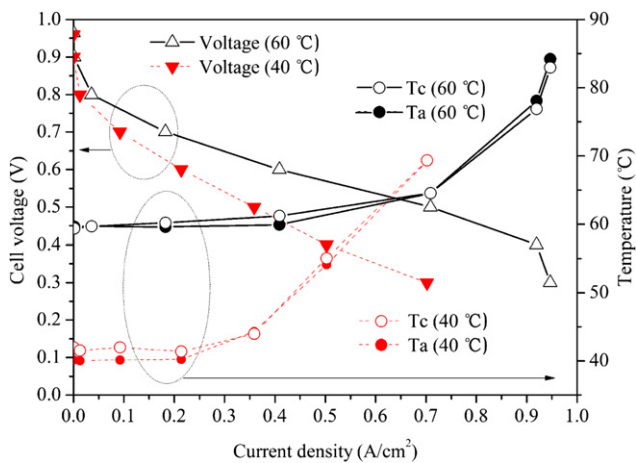


**Fig. 11 – Correlations among current densities, voltages and average temperatures on anode and cathode sides.**

temperatures of different cell components may have different relationship with current densities, and are also dependent on operating conditions.

**3.4. Temperature distribution behind the cathode FFP (CFFP)**

Immediately after the cell has operated for 6 h under a chosen voltage from 0.9 V to 0.3 V, temperature distributions over 100 units on the back side of the CFFP were obtained for the two initial cell temperatures. These temperature distributions over space maintained by cell itself are found to be entirely different under different operation conditions. In what follows, those temperature profiles under voltages of 0.5 V, 0.4 V and 0.3 V are analyzed. Figs. 12 and 13 present temperature isolines where red numerals are the local highest temperatures and contour with black numerals stands for the averaged value of the entire field. In the figures the temperature difference between two neighboring contours is 1 K, and black bold lines with arrows indicate oxygen flow paths from inlet to outlet.

A typical hydrogen PEMFC has relatively high power generation efficiency, at approximately 50%, which means the remaining 50% is waste heat [83]. This waste heat must be transferred through FFPs, current collectors and endplates to the environment to maintain cell normal operation. Thus, ensemble temperature distributions of the cell depend on the processes of electrochemistry, charge transports, heat transfer between layers and heat dissipation to the surroundings. The two major factors dominating temperature profiles are heat generation inside the cell and heat dissipation through the cell outside surface. The larger the outlet overall current is, the more the heat generation is. Under the natural convection cooling condition the capacity of heat dissipation to the surroundings is characterized by the temperature difference between the cell outer surfaces and the surroundings, and the higher the temperature difference, the more the heat dissipation.

Figs. 12 and 13 show that all the overall temperature levels increase as outlet voltages decrease, because a decrease in the outlet voltage is associated with an increase in the current density hence the average temperature as depicted in Fig. 11. Apart from this character, following three features may be noted.

Firstly, contour shapes of the isoline of the field averaged temperature distributions are similar at the same initial temperature. At the initial temperature of 60 °C, the areas surrounded by a specified higher temperature become slightly larger with the decrease of voltages, which means an increase in heat generation; while at 40 °C, little change of area surrounded by the average temperature occurs which means the equivalencies between heat generation and dissipation. From the temperature fields presented in Figs. 12 and 13, it can be observed that the temperature gradients at initial temperature of 40 °C are larger than those of 60 °C, which is an indication of the competitive relation between heat generation and heat dissipation.

Another distinctive feature in Figs. 12 and 13 is the non-uniformity of the temperature distributions, and these non-uniform temperature distributions often exhibit unequal trends according to initial temperature values. At initial

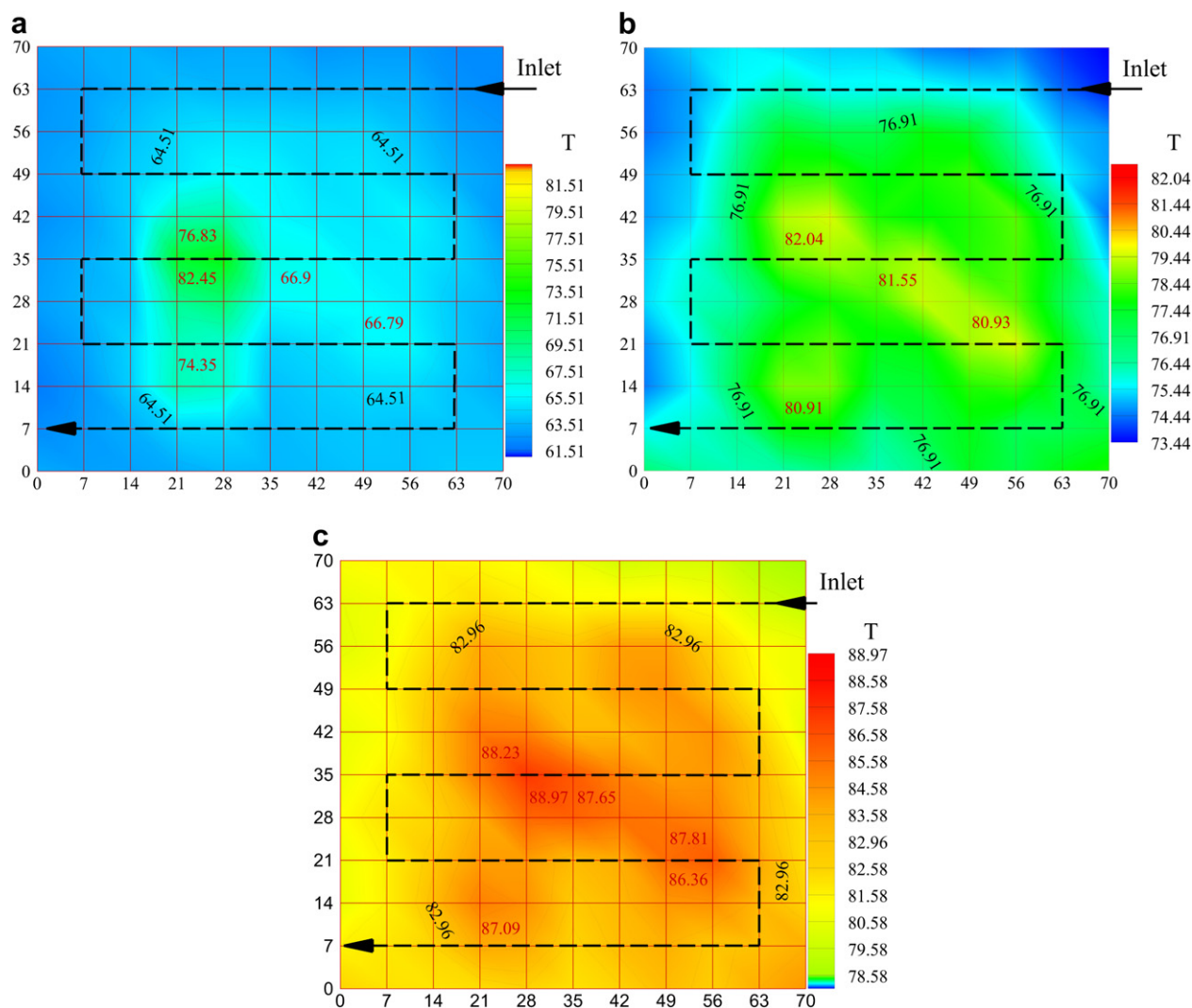


**Fig. 12** – Temperature distributions behind the cathode FFP with size of 70 mm × 70 mm under 60 °C: a) 0.5 V; b) 0.4 V; c) 0.3 V.

temperature of 60 °C, regions with local high temperature are “λ”-shaped approximately, while at 40 °C local high temperature regions become “T”-shaped roughly. Such non-uniform distribution of the local high temperature regions are mainly attributed to the existence of multiple local heat sources/sinks with different intensities inside a PEMFC, and different temperature distributions also show different distributions of heat sources/sinks under different operating conditions. According to Ref. [13] five heat sources/sinks exist inside a PEMFC, among which three kinds are dominated, i.e., heat source by activation loss, half-reactions and Joule effects. These three heat sources are influenced by many factors. From the test data obtained in the present study and the available knowledge about heat sources/sinks within fuel cell it is hard to convincingly explain why the high temperature regions at 40 °C and 60 °C exhibit such specific shape. However, one thing may be quite certain is that where the local current density is higher there must exist more heat [45]. Some additional explain to the high temperature regions will be provided in the following presentation.

The third common feature is that the high temperature regions are mainly located in the center part of the cell. This may be explained as follows. In our test the inlet oxygen is humidified slightly with 25% of relative humidity which makes membrane regions near inlet only partially humidified, resulting in high proton resistance across the membrane. Thus the local current densities near the inlet are dominated by proton conduction despite enough supply of the reactive gas. Along the gas flow path more water retention in the electrode occurs with the reaction progress, and electro-osmotic drag plays a significant role. Meanwhile the water dragged by the protons from the anode to cathode wets the membrane, as a result, the membrane resistance decreases, contributing to high local current densities and local temperatures where the reactive gas is fed sufficiently in the middle part of gas paths in Figs. 12 and 13. There are some minor differences between the two initial temperature cases. The overall gas velocity at initial temperature of 40 °C is lower than that of 60 °C at the same stoichiometry, resulting in a weaker drainage ability of liquid water for the case of initial

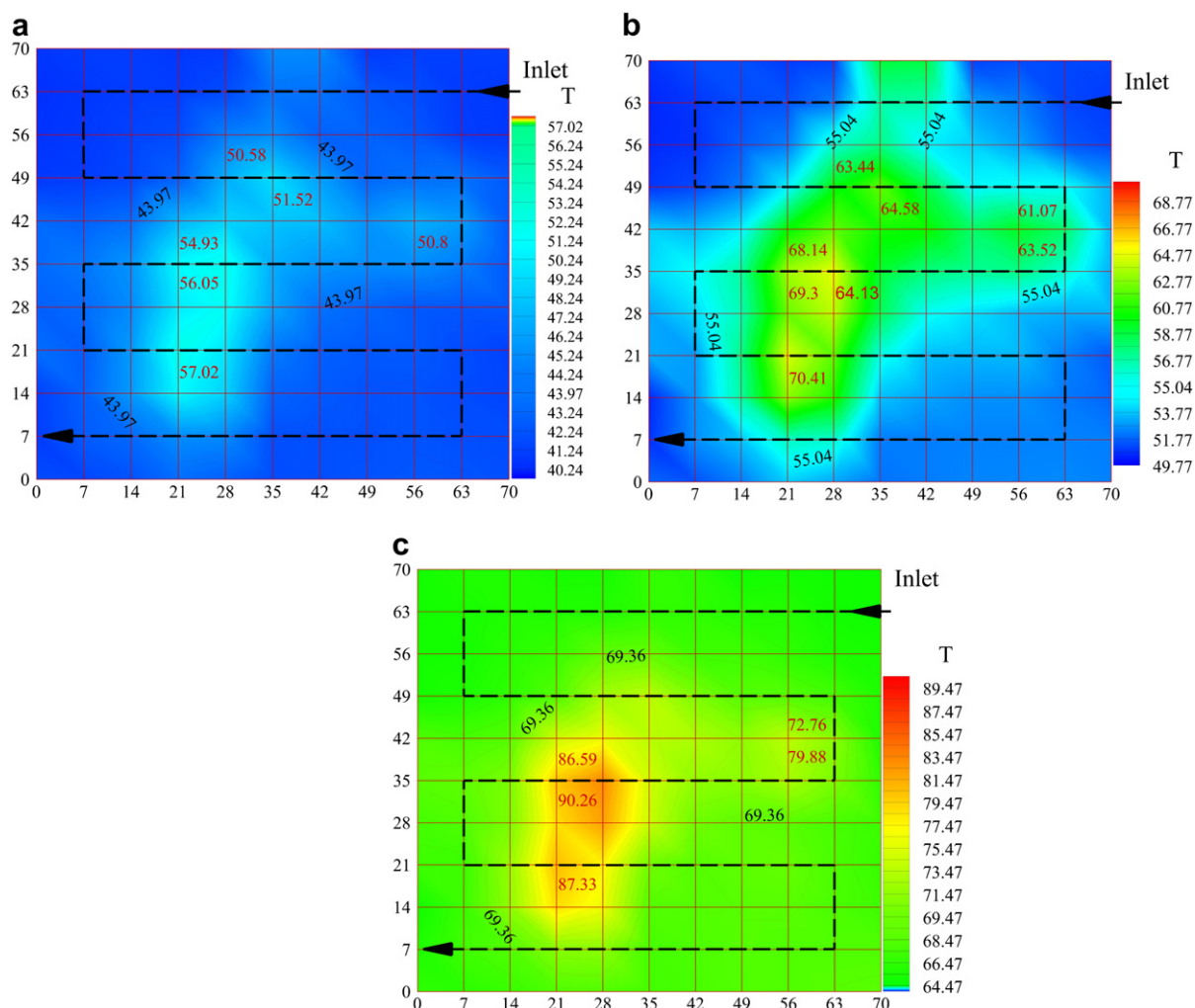


**Fig. 13** – Temperature distributions behind the cathode FFP with size of 70 mm × 70 mm under 40 °C: a) 0.5 V; b) 0.4 V; c) 0.3 V.

temperature of 40 °C. Thus the point where the membrane is full humidified at initial temperature of 40 °C is earlier than that of 60 °C, and this is witnessed by the earlier occurrence of the high local temperatures along the gas paths in Fig. 12 than that in Fig. 13. In addition, there exist local high temperatures on the corner from the second to the third parallel paths in Fig. 13 while this does not occur in Fig. 12. The corner high temperature might be caused by flow recirculation or stagnation around the corner, which makes a weaker drainage of liquid water in that local region.

On the repeated occurrence of the locally higher temperature regions along the gas flow paths shown in Figs. 12 and 13, it may be resulted from the dynamic balance between local membrane humidity and local temperature. It is well-known that even small variations in temperature have dramatic effects on saturation vapor pressure due to their exponential relation [84], so saturation vapor pressure increases rapidly with temperature elevation, resulting in a rapid water evaporation and a decrease in liquid water saturation. Consequently, the membrane resistance becomes larger due to bad membrane humidities, producing lower local current densities

and lower local temperatures. However, the decrease of local temperature may lead to an increase of liquid water saturation, making the local membrane being humidified better. As a result, high local temperature occurs with high local current densities. Maranzana et al. also concluded that the maximum current density corresponded probably with the point where the vapor saturation pressure was reached at the electrode [30]. The above-mentioned processes may take place cyclically, as long as the reactive gas is plentiful along the gas flow paths. In Figs. 12 and 13 the number of the full cycles is operation condition dependent: there are two full cycles at initial temperature of 60 °C seen from Figs. 12a–c, three full cycles at initial temperature of 40 °C and 0.5 V or 0.4 V in Figs. 13-a and 13-b, while two full cycles for the case of 40 °C and 0.3 V in Fig. 13-c.

As indicated earlier the above temperature distributions are on the back side of CFFP, with measuring points having a distance 1 mm to gas channels and 2 mm to MEA in the across-plane direction, thus, the measured temperature distributions may be approximately regarded as those of gas channel. Where local current densities are high, liquid water

trends to occur firstly in the electrode (GDL) and then in the gas channel, releasing a large amount of condensation heat with an equivalent order of half-reaction. The occurrence of liquid may deteriorate the uniformity of temperature distribution [12,43]. Although the place where liquid water appears in gas channel might not be the same in the electrode, they are expected to be close to each other. In our experiments after each test the fuel cell was detached and water stain regions were found sporadically in the cathode gas channel, basically in accordance with the high temperature zones measured in the test.

Lastly it should be noted that the details of the non-uniformity of temperature distributions found in our tests cannot be captured if the number of measuring points is not large enough.

### 3.5. Temperature distribution behind the anode FFP (AFFP)

Fig. 14 presents temperature variations along serpentine gas flow paths at the back side of the AFFP. At initial temperature of 60 °C, the maximum temperature difference ranges from 0.7 °C to 0.9 °C when the voltage are higher than 0.5 V, and the maximum temperature differences are 1.1 °C, 1.6 °C and 1.7 °C at 0.5 V, 0.4 V and 0.3 V, respectively. All these maximum temperature differences do not exceed 2 °C, not so significant as those in cathode side shown in Fig. 15.

Our measured results are qualitatively agreed well with those reported in literature for the temperature differences between different components or within the same component. For example, the temperature difference between gas channels of anode and cathode is about 3–4 °C [54]; At the cathode side: about 3 °C at moderate currents and 2 °C at high currents among GDL surface is found in [57]; While at the anode side: 8 °C of temperature difference exists in the surface of MEA after 60 s-runnig and 4.5–6 °C during 1800 s-testing [49], and 4 °C among five measure points on the surface of GDL [54]; Fuel cells with different operation controls and parts designs are tested in [47,48], and it is reported that all temperature differences are around or within 10 °C.

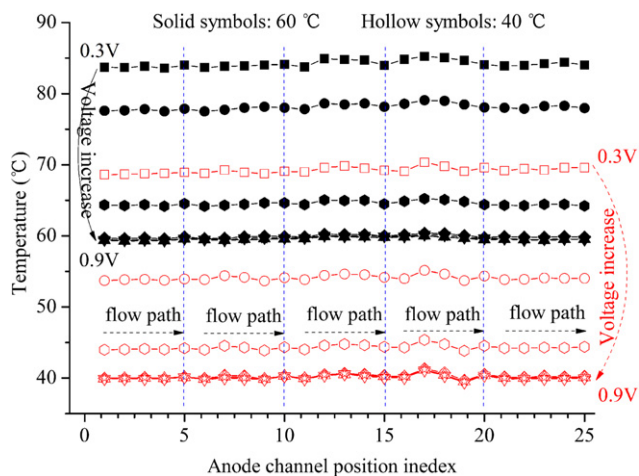


Fig. 14 – Temperature distributions along serpentine gas channels behind the anode FFP.

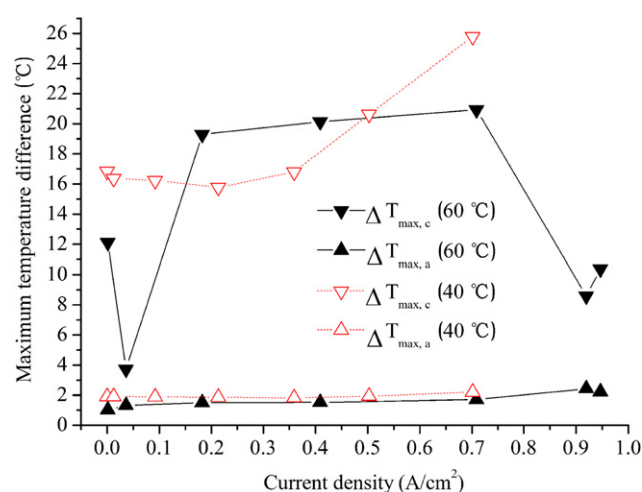


Fig. 15 – Maximum temperature difference as functions of current densities both on the cathode and anode side.

## 4. Conclusions

The temperature fields at the back sides of the cathode and anode flow field plates of a PEMFC at different preset initial temperatures and output voltages under natural cooling conditions were carefully determined and analyzed from the data obtained in the start-up period and the subsequent operational time as long as 20 thousands seconds. Following conclusions can be obtained:

- 1) Trends of anode temperatures changing with time differ during voltage jump under different operation conditions: overshoot behavior occurs at moderate current densities while asymptotic behavior happens for high current densities; and the temperature stable time also depends on operation conditions. Anode temperatures can reach quite relatively stable values or fluctuate around some relative stable plateaus, provided that the test period is long enough, being in the order of several thousand seconds for the cell tested.
- 2) Trends of the outlet current changing with time are more complex during voltage jump, with different dynamic behavior under different operation conditions. It takes more than 1500 s for the current to reach relatively stable levels at low voltage settings, and the outlet currents fluctuate within a certain range even during the latter 5 h. Furthermore, variations of the outlet currents with time are dependent on different internal conditions of cell, with somewhat periodic character being in common. These periodical trends with average intervals ranging from  $10^2$ – $10^3$  s, are suggested to be caused by the repeated formation, accumulation, and expulsion of liquid water in the cell.
- 3) There are some hystereses between anode temperatures and outlet currents, and the temperature lag behind currents due to the thermal inertia of cell is in the order of  $10$ – $10^3$  s. Such infer can be boldly made that those temperatures of different cell components may have different thermal behavior, correlating with current densities.

- 4) A 20 °C rise of the averaged temperatures on both sides of FFP above the initial temperature settings of the cell was found in the tested cell, indicating that the conventional polarization curves are actually obtained under rising temperature condition.
- 5) There exists non-uniformity of temperature distributions at the FFP back sides of both cathode and anode, with the non-uniformity of the cathode side being much larger than that of anode side (20 °C vs. 1–2 °C). However, the average temperatures of two back sides are quite close to each other with a difference only of 1–2 °C.

From the present test data and quite a few other experimental results for the fuel cell temperature distribution, it is obvious that much more work should be conducted to quantify and reveal: (1) what is the steady state of a fuel cell operation; (2) how to describe the thermal boundary condition of a fuel cell for numerical simulation; (3) how to improve the data reproducibility of fuel cell measurement, and (4) how to estimate the uncertainties of fuel cell measurements.

## Acknowledgments

The authors thank the supports of the National Natural Science Foundation of China (No. 51136004, No. 51176155).

## Nomenclature

$\lambda_1$	Thermal conductivity of the field flow plate, W/mK
$\lambda_2$	Thermal conductivity of the wire of thermocouple, W/mK
$\delta_1$	The thickness of the field flow plate, m
$\delta_2$	The length of the sheath of thermocouple, m
$\delta\tau_1$	Time that the temperature lags behind current while the current goes high, s
$\delta\tau_2$	Time that the temperature lags behind current while the current goes lower, s
$I_{\text{normal}}$	Dimensionless current density
$T_{\text{normal}}$	Dimensionless temperature
$T$	Temperature, °C
$T_c$	Cathode temperature, °C
$T_a$	Anode temperature, °C
$\Delta T_{\text{max}, c}$	Maximum temperature difference on the cathode side, °C
$\Delta T_{\text{max}, a}$	Maximum temperature difference on the anode side [°C]
$\Delta T_p$	Maximum temperature error in the measurement of surface [°C]
$\Delta T_{\text{sh}}$	Maximum temperature difference between the environment and the inner measuring point, °C

## REFERENCES

- [1] Weast RC, Astle MJ. CRC handbook of chemistry and physics: a ready-reference book of chemical and physical data 1981–1982. CRC Press Inc; 1981.
- [2] Bernardi DM, Verbrugge MW. A mathematical model of the solid-polymer-electrolyte fuel cell. *Journal of the Electrochemical Society* 1992;139:2477–91.
- [3] Stockie JM, Promislow K, Wetton BR. A finite volume method for multicomponent gas transport in a porous fuel cell electrode. *International Journal for Numerical Methods in Fluids* 2003;41:577–99.
- [4] Kim S, Mench MM. Investigation of temperature-driven water transport in polymer electrolyte fuel cell: thermo-osmosis in membranes. *Journal of Membrane Science* 2009; 328:113–20.
- [5] Lee C-I, Chu H-S. Effects of temperature on the location of the gas–liquid interface in a PEM fuel cell. *Journal of Power Sources* 2007;171:718–27.
- [6] Afshari E, Jazayeri S, Mollayi Barzi Y. Effect of water phase change on temperature distribution in proton exchange membrane fuel cells. *Heat and Mass Transfer* 2010;46:1295–305.
- [7] Santarelli MG, Torchio MF, Cochis P. Parameters estimation of a PEM fuel cell polarization curve and analysis of their behavior with temperature. *Journal of Power Sources* 2006; 159:824–35.
- [8] Zhang J, Tang Y, Song C, Zhang J, Wang H. PEM fuel cell open circuit voltage (OCV) in the temperature range of 23 °C to 120 °C. *Journal of Power Sources* 2006;163:532–7.
- [9] Newman JS. *Electrochemical systems*. Englewood Cliffs: Prentice-Hall; 1973.
- [10] Song C, Tang Y, Zhang JL, Zhang J, Wang H, Shen J, et al. PEM fuel cell reaction kinetics in the temperature range of 23–120 °C. *Electrochimica Acta* 2007;52:2552–61.
- [11] Vie PJS, Kjelstrup S. Thermal conductivities from temperature profiles in the polymer electrolyte fuel cell. *Electrochimica Acta* 2004;49:1069–77.
- [12] Abdullah AM, Okajima T, Mohammad AM, Kitamura F, Ohsaka T. Temperature gradients measurements within a segmented H<sub>2</sub>/air PEM fuel cell. *Journal of Power Sources* 2007;172:209–14.
- [13] Ramousse J, Lottin O, Didierjean S, Maillet D. Heat sources in proton exchange membrane (PEM) fuel cells. *Journal of Power Sources* 2009;192:435–41.
- [14] Pharoah JG, Burheim OS. On the temperature distribution in polymer electrolyte fuel cells. *Journal of Power Sources* 2010; 195:5235–45.
- [15] Matian M, Marquis A, Brandon N. Model based design and test of cooling plates for an air-cooled polymer electrolyte fuel cell stack. *International Journal of Hydrogen Energy* 2011;36:6051–66.
- [16] Herrera OE, Wilkinson DP, Mérida W. Anode and cathode overpotentials and temperature profiles in a PEMFC. *Journal of Power Sources* 2012;198:132–42.
- [17] Jung G-B, Lo K-F, Su A, Weng F-B, Tu C-H, Yang T-F, et al. Experimental evaluation of an ambient forced-feed air-supply PEM fuel cell. *International Journal of Hydrogen Energy* 2008;33:2980–5.
- [18] Choi K-S, Kim H-M, Yoon HC, Forrest ME, Erickson PA. Effects of ambient temperature and relative humidity on the performance of Nexa fuel cell. *Energy Conversion and Management* 2008;49:3505–11.
- [19] Yuan X, Sun JC, Blanco M, Wang H, Zhang J, Wilkinson DP. AC impedance diagnosis of a 500 W PEM fuel cell stack: part I: stack impedance. *Journal of Power Sources* 2006;161:920–8.
- [20] Andreasen SJ, Jespersen JL, Schaltz E, Kær SK. Characterisation and modelling of a high temperature PEM fuel cell stack using electrochemical impedance spectroscopy. *Fuel Cells* 2009;9:463–73.
- [21] Lee HI, Lee CH, Oh TY, Choi SG, Park IW, Baek KK. Development of 1 kW class polymer electrolyte membrane fuel cell power generation system. *Journal of Power Sources* 2002;107:110–9.

- [22] Adzakpa KP, Ramousse J, Dubé Y, Akremi H, Agbossou K, Dostie M, et al. Transient air cooling thermal modeling of a PEM fuel cell. *Journal of Power Sources* 2008;179:164–76.
- [23] Gao F, Blunier B, Miraoui A, El-Moudni A. Cell layer level generalized dynamic modeling of a PEMFC stack using VHDL-AMS language. *International Journal of Hydrogen Energy* 2009;34:5498–521.
- [24] Gao F, Blunier B, Miraoui A, El-Moudni A. Proton exchange membrane fuel cell multi-physical dynamics and stack spatial non-homogeneity analyses. *Journal of Power Sources* 2010;195:7609–26.
- [25] Mench MM, Burford DJ, Davis TW. In situ temperature distribution measurement in an operating polymer electrolyte fuel cell. Washington, D.C., USA: ASME International Mechanical Engineering Congress, Heat Transfer Division; 2003. p. 415–28.
- [26] Wilkinson M, Blanco M, Gu E, Martin JJ, Wilkinson DP, Zhang JJ, et al. In situ experimental technique for measurement of temperature and current distribution in proton exchange membrane fuel cells. *Electrochemical and Solid-State Letters* 2006;9: A507-AA11.
- [27] Lee S-K, Ito K, Ohshima T, Noda S, Sasaki K. In situ measurement of temperature distribution across a proton exchange membrane fuel cell. *Electrochemical and Solid-State Letters* 2009;12: B126-BB30.
- [28] Zhang G, Guo L, Ma L, Liu H. Simultaneous measurement of current and temperature distributions in a proton exchange membrane fuel cell. *Journal of Power Sources* 2010;195: 3597–604.
- [29] Wen C-Y, Huang G-W. Application of a thermally conductive pyrolytic graphite sheet to thermal management of a PEM fuel cell. *Journal of Power Sources* 2008;178:132–40.
- [30] Maranzana G, Lottin O, Colinart T, Chupin S, Didierjean S. A multi-instrumented polymer exchange membrane fuel cell: observation of the in-plane non-homogeneities. *Journal of Power Sources* 2008;180:748–54.
- [31] Jiao K, Alaefour IE, Karimi G, Li X. Simultaneous measurement of current and temperature distributions in a proton exchange membrane fuel cell during cold start processes. *Electrochimica Acta* 2011;56:2967–82.
- [32] He S, Mench MM, Tadigadapa S. Thin film temperature sensor for real-time measurement of electrolyte temperature in a polymer electrolyte fuel cell. *Sensors and Actuators A: Physical* 2006;125:170–7.
- [33] Lee C-Y, Lee S-J, Hu Y-C, Shih W-P, Fan W-Y, Chuang C-W. Real time monitoring of temperature of a micro proton exchange membrane fuel cell. *Sensors* 2009;9:1423–32.
- [34] Lee C-Y, Fan W-Y, Hsieh W-J. In-situ monitoring of internal local temperature and voltage of Proton exchange membrane fuel cells. *Sensors* 2010;10:6395–405.
- [35] Lee C-Y, Chan P-C, Lee C-J. Use of multi-functional flexible micro-sensors for in situ measurement of temperature, voltage and fuel flow in a proton exchange membrane fuel cell. *Sensors* 2010;10:11605–17.
- [36] Lee C-Y, Fan W-Y, Chang C-P. A novel method for in-situ monitoring of local voltage, temperature and humidity distributions in fuel cells using flexible multi-functional micro sensors. *Sensors* 2011;11:1418–32.
- [37] Lee C-Y, Weng F-B, Cheng C-H, Shiu H-R, Jung S-P, Chang W-C, et al. Use of flexible micro-temperature sensor to determine temperature in situ and to simulate a proton exchange membrane fuel cell. *Journal of Power Sources* 2011; 196:228–34.
- [38] Lee C-Y, Lee S-J, Wu G-W. Measuring of temperature and humidity within the membrane electrode assembly by micro-sensors. In: Hinduja S, Fan K-C, editors. *Proceedings of the 35th international MATADOR conference*. London: Springer; 2007. p. 377–80.
- [39] Lee C-Y, Wu G-W, Hsieh C-L. In situ diagnosis of micrometallic proton exchange membrane fuel cells using microsensors. *Journal of Power Sources* 2007;172:363–7.
- [40] Lee C-Y, Hsieh W-J, Wu G-W. Embedded flexible microsensors in MEA for measuring temperature and humidity in a micro-fuel cell. *Journal of Power Sources* 2008;181:237–43.
- [41] Lee C-Y, Lin C-H. A novel integration approach for combining the micro thermal sensor and stainless steel foil as gas diffusion layer in micro fuel cell. *Renewable Energy* 2010;35:759–62.
- [42] Wang MH, Guo H, Ma CF, Ye F, Yu J, Liu X, et al. Temperature measurement technologies and their application in the research of fuel cells. First international conference on fuel cell science, engineering and technology. Rochester, NY, USA 2003. p. 95–100.
- [43] Hakenjos A, Muentner H, Wittstadt U, Hebling C. A PEM fuel cell for combined measurement of current and temperature distribution, and flow field flooding. *Journal of Power Sources* 2004;131:213–6.
- [44] Shimoi R, Masuda M, Fushinobu K, Kozawa Y, Okazaki K. Visualization of the membrane temperature field of a polymer electrolyte fuel cell. *Journal of Energy Resources Technology* 2004;126:258–61.
- [45] Hakenjos A, Hebling C. Spatially resolved measurement of PEM fuel cells. *Journal of Power Sources* 2005;145:307–11.
- [46] Chikahisa T, Tabe Y, Kikuta K, Nohara N, Shinohara H. Measurement of water production behavior, temperature, and current density distributions in a polymer electrolyte fuel cell. *ASME Conference Proceedings*. 2006: pp. 25–30.
- [47] Nishimura A, Shibuya K, Morimoto A, Tanaka S, Hirota M, Nakamura Y, et al. In-situ measurement of in-plane temperature distribution in a single-cell polymer electrolyte fuel cell using thermograph. *Journal of Environment and Engineering* 2011;6:1–16.
- [48] Nishimura A, Shibuya K, Morimoto A, Tanaka S, Hirota M, Nakamura Y, et al. Dominant factor and mechanism of coupling phenomena in single cell of polymer electrolyte fuel cell. *Applied Energy* 2012;90:73–9.
- [49] Wang M, Guo H, Ma C. Temperature distribution on the MEA surface of a PEMFC with serpentine channel flow bed. *Journal of Power Sources* 2006;157:181–7.
- [50] Basu S, Renfro MW, Gorgun H, Cetegen BM. In situ simultaneous measurements of temperature and water partial pressure in a PEM fuel cell under steady state and dynamic cycling. *Journal of Power Sources* 2006;159:987–94.
- [51] Basu S, Renfro MW, Cetegen BM. Spatially resolved optical measurements of water partial pressure and temperature in a PEM fuel cell under dynamic operating conditions. *Journal of Power Sources* 2006;162:286–93.
- [52] Basu S, Xu H, Renfro MW, Cetegen BM. In situ optical diagnostics for measurements of water vapor partial pressure in a PEM fuel cell. *Journal of Fuel Cell Science and Technology* 2006;3:1–7.
- [53] Sur R, Boucher TJ, Renfro MW, Cetegen BM. In situ measurements of water vapor partial pressure and temperature dynamics in a PEM fuel cell. *Journal of the Electrochemical Society* 2010;157:B45–53.
- [54] Hinds G, Stevens M, Wilkinson J, de Podesta M, Bell S. Novel in situ measurements of relative humidity in a polymer electrolyte membrane fuel cell. *Journal of Power Sources* 2009;186:52–7.
- [55] David NA, Wild PM, Hu J, Djilali N. In-fibre Bragg grating sensors for distributed temperature measurement in a polymer electrolyte membrane fuel cell. *Journal of Power Sources* 2009;192:376–80.
- [56] David NA, Wild PM, Jensen J, Navessin T, Djilali N. Simultaneous in situ measurement of temperature and relative humidity in a PEMFC using optical fiber sensors.

- Journal of the Electrochemical Society 2010;157: B1173-B11B9.
- [57] Inman K, Wang X, Sangeorzan B. Design of an optical thermal sensor for proton exchange membrane fuel cell temperature measurement using phosphor thermometry. *Journal of Power Sources* 2010;195:4753–7.
- [58] Moxley JF, Tulyani S, Benziger JB. Steady-state multiplicity in the autohumidification polymer electrolyte membrane fuel cell. *Chemical Engineering Science* 2003;58:4705–8.
- [59] Benziger J, Chia E, Karnas E, Moxley J, Teuscher C, Kevrekidis IG. The stirred tank reactor polymer electrolyte membrane fuel cell. *AIChE Journal* 2004;50:1889–900.
- [60] Benziger J, Chia E, Moxley JF, Kevrekidis IG. The dynamic response of PEM fuel cells to changes in load. *Chemical Engineering Science* 2005;60:1743–59.
- [61] Chia E-SJ, Benziger JB, Kevrekidis IG. STR-PEM fuel cell as a reactor building block. *AIChE Journal* 2006;52:3902–10.
- [62] Benziger J. Fan the flame with water: current ignition, front propagation and multiple steady states in polymer electrolyte membrane fuel cells. *AIChE Journal* 2009;55: 3034–40.
- [63] He G, Yamazaki Y, Abudula A. A three-dimensional analysis of the effect of anisotropic gas diffusion layer(GDL) thermal conductivity on the heat transfer and two-phase behavior in a proton exchange membrane fuel cell(PEMFC). *Journal of Power Sources* 2010;195:1551–60.
- [64] Nam J, Chippar P, Kim W, Ju H. Numerical analysis of gas crossover effects in polymer electrolyte fuel cells (PEFCs). *Applied Energy* 2010;87:3699–709.
- [65] Yuan W, Tang Y, Pan M, Li Z, Tang B. Model prediction of effects of operating parameters on proton exchange membrane fuel cell performance. *Renewable Energy* 2010;35: 656–66.
- [66] Jiao K, Li X. Cold start analysis of polymer electrolyte membrane fuel cells. *International Journal of Hydrogen Energy* 2010;35:5077–94.
- [67] Hua M. Numerical studies of liquid water behaviors in PEM fuel cell cathode considering transport across different porous layers. *International Journal of Hydrogen Energy* 2010;35:5569–79.
- [68] Pengtao S. Modeling studies and efficient numerical methods for proton exchange membrane fuel cell. *Computer Methods in Applied Mechanics and Engineering* 2011;200:3324–40.
- [69] Wu H-W, Ku H- W. The optimal parameters estimation for rectangular cylinders installed transversely in the flow channel of PEMFC from a three-dimensional PEMFC model and the Taguchi method. *Applied Energy* 2011;88:4879–90.
- [70] Berning T, Odgaard M, Kær SK. Water balance simulations of a polymer-electrolyte membrane fuel cell using a two-fluid model. *Journal of Power Sources* 2011;196:6305–17.
- [71] Catlin G, Advani SG, Prasad AK. Optimization of polymer electrolyte membrane fuel cell flow channels using a genetic algorithm. *Journal of Power Sources* 2011;196:9407–18.
- [72] Ramos-Alvarado B, Hernandez-Guerrero A, Juarez-Robles D, Li P. Numerical investigation of the performance of symmetric flow distributors as flow channels for PEM fuel cells. *International Journal of Hydrogen Energy* 2012;37: 436–48.
- [73] Matian M, Marquis A, Brett D, Brandon N. An experimentally validated heat transfer model for thermal management design in polymer electrolyte membrane fuel cells. *Proceedings of the Institution of Mechanical Engineers, Part A: Journal of Power and Energy* 2010;224:1069–81.
- [74] <http://www.matweb.com>.
- [75] <http://www.splusplus.com>.
- [76] <http://www.arbin.com>.
- [77] Cuccaro R, Lucariello M, Battaglia A, Graizzaro A. Research of a HySyLab internal standard procedure for single PEMFC. *International Journal of Hydrogen Energy* 2008;33:3159–66.
- [78] Divisek J. Low temperature fuel cells. In: *Handbook of fuel cells*. John Wiley & Sons, Ltd; 2010.
- [79] Zenith F, Skogestad S. Control of the mass and energy dynamics of polybenzimidazole-membrane fuel cells. *Journal of Process Control* 2009;19:415–32.
- [80] Kim S, Shimpalee S, Van Zee JW. The effect of stoichiometry on dynamic behavior of a proton exchange membrane fuel cell (PEMFC) during load change. *Journal of Power Sources* 2004;135:110–21.
- [81] Atkins JR, Savett SC, Creager SE. Large-scale current fluctuations in PEM fuel cells operating with reduced feed stream humidification. *Journal of Power Sources* 2004;128:201–7.
- [82] Sanchez DG, Diaz DG, Hiesgen R, Wehl I, Friedrich KA. Oscillations of PEM fuel cells at low cathode humidification. *Journal of Electroanalytical Chemistry* 2010;649:219–31.
- [83] Faghri A, Guo Z. Challenges and opportunities of thermal management issues related to fuel cell technology and modeling. *International Journal of Heat and Mass Transfer* 2005;48:3891–920.
- [84] Larminie J, Dicks A. *Fuel cell systems explained*. New York: Wiley; 2000.